AUT Journal of Mathematics and Computing

AUT J. Math. Com., 1(1) (2020) 1-15
DOI: 10.22060/ajmc.2019.15990.1019

A meshless numerical investigation based on the RBF-QR approach for elasticity problems

Mostafa Abbaszadeh*[a], Mehdi Dehghan[b]

[a]Department of Mathematics and Computer Science, Amirkabir University of Technology, 424, Hafez Ave., Tehran 15914, Iran
[b]Department of Mathematics and Computer Science, Amirkabir University of Technology, 424, Hafez Ave., Tehran 15914, Iran

ABSTRACT: In the current research work, we present an improvement of meshless boundary element method (MBEM) based on the shape functions of radial basis functions-QR (RBF-QR) for solving the two-dimensional elasticity problems. The MBEM has benefits of the boundary integral equations (BIEs) to reduce the dimension of problem and the meshless attributes of moving least squares (MLS) approximations. Since the MLS shape functions don't have the delta function property, applying boundary conditions is not simple. Here, we propose the MBEM using RBF-QR to increase the accuracy and efficiency of MBEM. To show the performance of the new technique, the two-dimensional elasticity problems have been selected. We solve the mentioned model on several irregular domains and report simulation results.

Review History:

Received:13 January 2019
Revised:18 April 2019
Accepted:24 April 2019
Available Online:1 February 2020

Keywords:

Boundary element method
RBF-QR approach
Two-dimensional elasticity problems
Meshless method

1. Introduction

Recently, the meshless methods have attracted many attentions to simulate the most phenomena in natural science [25, 26]. The meshless methods don't require any mesh. The meshless approach has been employed in boundary integral equations (BIEs) such as boundary node method (BNM) [14, 34], boundary element method [36, 37, 38, 39] and the hybrid boundary node method [51]. These methods are based on the discretization of the boundary problem. For example, the boundary element method is a meshless method that discretizes the boundary of problem [9, 10, 11]. The boundary node techniques employ the moving least-squares (MLS) approximation for the test and trial functions. The main advantage of these methods is reducing the dimension of problem one less. Also, since the MLS shape functions lack the delta function, the boundary conditions can not be applied with more accuracy as this is the main defect of these methods. For overcoming the mentioned issue Li and Zhu [19] employed the improved MLS approximation [24] in boundary node method to overcome the explained problem. The main aim of [27] is to present a very important and unique property of the linearly conforming point interpolation method (LC-PIM). Also, author of [33] proposed the direct meshless Local Petrov-Galerkin (DMLPG) method for solving elasto-static problems.

Authors of [18] formulated and implemented a new improved complex variable element-free Galerkin (ICVEFG) method for solving two-dimensional large deformation problems of elastoplasticity in total Lagrangian description. The main aim of [3] is developing the complex variable reproducing kernel particle method (CVRKPM) for solving the bending problems of isotropic thin plates on elastic foundations. Based on the interpolating moving least-squares (IMLS) method a novel improved element-free Galerkin (IEFG) method has been proposed in [4] for solving nonlinear elastic large deformation problems. In [31], the authors presented the dimension split element-free

*Corresponding author.
E-mail addresses: m.abbaszadeh@aut.ac.ir, mdehghan@aut.ac.ir

Galerkin (DSEFG) method for three-dimensional potential problems as the main purpose of the DSEFG method is transforming a three-dimensional potential problem into a series of two-dimensional problems.

The main aim of the current paper is to apply a new meshless boundary element method (MBEM) based on the shape functions of RBF-QR approach to simulate the multi-dimensional elasticity problems. The shape functions of RBF-QR have been combined with a variational formulation of BIEs. The shape functions of RBF-QR are employed as the test and trial functions of the variational form. The shape functions of RBF-QR approach have spectral accuracy thus the accuracy of MBEM will be increased. The multi-dimensional Vlasov-Poisson and Vlasov-Poisson–Fokker–Planck systems have been solved by using the RKPM method in [6]. Also, the improved meshless methods are used in [7, 8] to simulate some models in fluid dynamics such as incompressible Navier–Stokes and compressible Euler equations.

In this manuscript, we consider two-dimensional elasticity problems in solid mechanics that are solved by meshless methods [1, 3, 15, 28]. Also, this model has been solved by finite element approximation [16], adaptive finite element-boundary element method [12], improved complex variable element free Galerkin method [5, 18], the complex variable element-free Galerkin (CVEFG) method [35], local boundary integral equation method [40] and etc. The GBNM has been employed for many problems, for example, potential theory [20, 52], Stokes flow [21, 22, 23, 43], 2D crack problems [44], magneto-hydrodynamic (MHD) equation [45], 2D elasticity [29, 32, 48] and Kirchhoff plates [49]. The RBF-QR method produces a new class of shape functions based on the Gaussian radial basis functions with spectral accuracy. This method is presented by Forenberg, Larsson and their co-workers [13, 17]. Authors of [30] developed a new version of interpolating moving least-squares (IMLS) method to apply it in the boundary element-free method (BEFM) for solving elasticity problems.
In this paper, we consider the following equation [50]

$$\nabla \cdot \boldsymbol{\sigma} + \mathbf{b} = 0, \qquad in \;\; \Omega,$$

in which

- ∇ is the divergence operator,
- $\boldsymbol{\sigma}$ is the stress tensor,
- $\mathbf{b}$ is the body force,
- Ω is the computational domain.

The boundary conditions for the above equation are [50]

$$\mathbf{u}(x,y) = \widetilde{\mathbf{u}}(x,y), \qquad (x,y) \in \Gamma_D,$$

$$\mathbf{t}(x,y) = \boldsymbol{\sigma}(x,y) \cdot \mathbf{n} = \widetilde{\mathbf{t}}(x,y), \qquad (x,y) \in \Gamma_N,$$

where

- $\mathbf{u}(x,y)$ is the displacement vector,
- $\widetilde{\mathbf{u}}(x,y)$ is the displacement vector on Γ_D,
- $\mathbf{t}(x,y)$ is the traction vector,
- $\widetilde{\mathbf{t}}(x,y)$ is traction vector on Γ_N,
- $\mathbf{n}$ is unit outward normal to $\Gamma = \Gamma_D \bigcup \Gamma_N$.

The strain and stress-strain for two-dimensional elasticity problems, respectively, are [50]

$$\boldsymbol{\varepsilon} = \nabla \mathbf{u},$$

$$\boldsymbol{\sigma} = \mathbf{D}\boldsymbol{\varepsilon},$$

in which $\mathbf{D}$ for a plane strain problem is

$$\mathbf{D} = \frac{E}{1-v^2}\left[\begin{array}{ccc} 1 & v & 0 \\ v & 1 & 0 \\ 0 & 0 & \frac{1-v}{2} \end{array}\right],$$

and for a plane stress problem is

$$\mathbf{D} = \frac{E}{(1+v)(1-2v)} \begin{bmatrix} 1-v & v & 0 \\ v & 1-v & 0 \\ 0 & 0 & \frac{1-2v}{2} \end{bmatrix}.$$

Also, in the above formula E is the Young's modulus and v is the Poisson's ratio.

2. RBF-QR shape functions

This is clear that the direct RBFs method has ill-conditioned interpolation matrix. Larsson et al [17] and Forenberg with his co-workers [13] proposed a new class of well-posed shape functions to overcome this important issue and to obtain more accurate numerical results. Here, we present some explanations on the RBF-QR method however the interested readers can refer to [13, 17] to find more information.

We approximate the Gaussian functions as follows [13, 17]

$$e^{-\varepsilon^2\|x-x_k\|^2} = \sum_{j=0}^{\infty} \varepsilon^{2j} c_j(x_k) e^{-\varepsilon^2 x^2} T_j(x), \tag{2.1}$$

in which $T_j(x)$ are Chebyshev functions and [13, 17]

$$c_j(x_k) = \frac{2t_j}{j!} e^{-\varepsilon^2 x_k^2} x_k^j \, {}_0F_1\left(; j+1; \varepsilon^k x_k^2\right), \qquad t_0 = \frac{1}{2}, \quad t_j = 1, \quad j > 0.$$

Also, in the above equation ${}_0F_1$ is hypergeometric function that is defined as

$$F_1\left(; a; z\right) = \sum_{n=0}^{\infty} \frac{z^n}{an!}.$$

Now, we consider

$$\phi\left(|x-x_j|\right) = e^{-\varepsilon^2 |x-x_k|^2},$$

and we collocate p terms of right hand side Eq. (2.1) at points $\{x_1, x_2, \ldots, x_N\}$ then we have [13, 17]

$$\underbrace{\begin{bmatrix} \phi\left(|x-x_1|\right) \\ \phi\left(|x-x_2|\right) \\ \vdots \\ \phi\left(|x-x_N|\right) \end{bmatrix}}_{\overrightarrow{\Phi}(x)} = \underbrace{\begin{bmatrix} c_0(x_1) & \varepsilon^2 c_1(x_1) & \ldots & \varepsilon^{2p} c_p(x_1) \\ c_0(x_2) & \varepsilon^2 c_1(x_2) & \ldots & \varepsilon^{2p} c_p(x_2) \\ \vdots & \vdots & \ddots & \vdots \\ c_0(x_N) & \varepsilon^2 c_p(x_N) & \ldots & \varepsilon^{2p} c_p(x_N) \end{bmatrix}_{N\times(p+1)}}_{M} \underbrace{\begin{bmatrix} e^{-\varepsilon^2 x^2} T_0(x) \\ e^{-\varepsilon^2 x^2} T_1(x) \\ \vdots \\ e^{-\varepsilon^2 x^2} T_p(x) \end{bmatrix}_{(p+1)\times 1}}_{\overrightarrow{N}(x)}.$$

Using the QR decomposition for matrix M we can get [13, 17]

$$\begin{aligned} \mathbf{M} = \mathbf{QR} \quad &= \quad \mathbf{Q} \begin{bmatrix} m_{1,1} & \varepsilon^2 m_{1,2} & \ldots & \varepsilon^{2p} m_{1,p+1} \\ 0 & \varepsilon^2 m_{2,2} & \ldots & \varepsilon^{2p} m_{2,p+1} \\ \vdots & \vdots & \ddots & \vdots \\ 0 & 0 & \ldots & \varepsilon^{2p} m_{n,p+1} \end{bmatrix} \\ &= \quad \mathbf{Q} \underbrace{\begin{bmatrix} 1 & 0 & \ldots & 0 \\ 0 & \varepsilon^2 & \ldots & \vdots \\ \vdots & \ldots & \ddots & 0 \\ 0 & \ldots & 0 & \varepsilon^{2p} \end{bmatrix}}_{\mathbf{E}} \begin{bmatrix} m_{1,1} & \varepsilon^2 m_{1,2} & \ldots & \varepsilon^{2p} m_{1,p+1} \\ 0 & m_{2,2} & \ldots & \varepsilon^{2(p-1)} m_{2,p+1} \\ \vdots & \vdots & \ddots & \vdots \\ 0 & 0 & \ldots & m_{n,p+1} \end{bmatrix}. \end{aligned}$$

$$
\begin{aligned}
\mathbf{A} &= \begin{bmatrix} \phi(x_1) \\ \phi(x_2) \\ \vdots \\ \phi(x_N) \end{bmatrix} = \begin{bmatrix} \phi(|x_1-x_1|) & \phi(|x_1-x_1|) & \dots & \phi(|x_1-x_1|) \\ \phi(|x_2-x_1|) & \phi(|x_2-x_1|) & \dots & \phi(|x_2-x_1|) \\ \vdots & \vdots & \ddots & \vdots \\ \phi(|x_N-x_1|) & \phi(|x_N-x_1|) & \dots & \phi(|x_N-x_1|) \end{bmatrix} \\
&= \begin{bmatrix} e^{-\varepsilon^2 x_1^2} T_0(x_1) & e^{-\varepsilon^2 x_1^2} T_1(x_1) & \dots & e^{-\varepsilon^2 x_1^2} T_p(x_1) \\ e^{-\varepsilon^2 x_2^2} T_0(x_2) & e^{-\varepsilon^2 x_2^2} T_1(x_2) & \dots & e^{-\varepsilon^2 x_2^2} T_p(x_2) \\ \vdots & \vdots & \ddots & \vdots \\ e^{-\varepsilon^2 x_N^2} T_0(x_N) & e^{-\varepsilon^2 x_N^2} T_1(x_N) & \dots & e^{-\varepsilon^2 x_N^2} T_p(x_N) \end{bmatrix} \mathbf{R}^T \mathbf{E}^T \mathbf{Q}^T.
\end{aligned}
$$

As a result, we have [13, 17]

$$\mathbf{A} = \mathbf{N}^T \mathbf{R}^T \mathbf{E}^T \mathbf{Q}^T.$$

We refer any interested readers for more information to papers [13, 17].

3. New meshless boundary element method

At first, we consider the following boundary integral equation based on the load point ϑ in which inside Ω, we have

$$u_i(\vartheta) = \int_\Gamma u_{ji}^*(\vartheta, \mathbf{x}) t_j(\mathbf{x}) d\Gamma - \int_\Gamma t_{ij}^*(\vartheta, \mathbf{x}) u_j(\mathbf{x}) d\Gamma + \int_\Omega u_{ij}^*(\vartheta, \mathbf{x}) f_j(\mathbf{x}) d\Omega.$$

Also

$$\Theta_{ij}(\vartheta) u_j(\vartheta) = \int_\Gamma u_{ij}^*(\vartheta, \mathbf{x}) t_j(\mathbf{x}) d\Gamma - \int_\Gamma t_{ij}^*(\vartheta, \mathbf{x}) u_j(\mathbf{x}) d\Gamma + \int_\Omega u_{ij}^*(\vartheta, \mathbf{x}) f_j(\mathbf{x}) d\Omega, \tag{3.1}$$

where ϑ is located on the boundary Γ and Θ_{ij} is the function of the internal angle. Also, u_{ij}^* and t_{ij}^* chosen as the displacement and the traction of Kelvin's solution, are the jth components of the displacement and traction due to a unit load in the x_i direction.

Let the boundary Γ be divided by sub-domains Γ_m for $m = 1, 2, \dots, N$. So

$$\Gamma = \bigcup_{m=1}^N \Gamma_m.$$

Now, Eq. (3.1) can be rewritten as follows

$$\Theta_{ki}(\vartheta) u_i(\vartheta) = \sum_{m=1}^N \int_{\Gamma_m} u_{ki}^*(\vartheta, \mathbf{x}) t_i(\mathbf{x}) d\Gamma - \sum_{m=1}^N \int_{\Gamma_m} t_{ki}^*(\vartheta, \mathbf{x}) u_i(\mathbf{x}) d\Gamma. \tag{3.2}$$

We consider some points on each sub-domain that the influence domain of each node is constructed. Let

$$u_i(\mathbf{x}) = \sum_{p=1}^{n_p} \phi_p(\mathbf{x}) u_i(\mathbf{x}_p),$$

$$t_i(\mathbf{x}) = \sum_{p=1}^{n_p} \phi_p(\mathbf{x}) t_i(\mathbf{x}_p).$$

Thus, Eq. (3.2) will be

$$\Theta_{ki}(\vartheta_q) u_i(\vartheta_q) = \sum_{m=1}^N \int_{\Gamma_m} u_{ki}^*(\vartheta_q, \mathbf{x}) \sum_{p=1}^{n_p} \phi_p(\mathbf{x}) t_i(\mathbf{x}_p) d\Gamma - \sum_{m=1}^N \int_{\Gamma_m} t_{ki}^*(\vartheta, \mathbf{x}) \sum_{p=1}^{n_p} \phi_p(\mathbf{x}) u_i(\mathbf{x}_p) d\Gamma, \tag{3.3}$$

in which ϑ_q are nodes and n_p is the number of nodes in each sub-domain. By applying the numerical integration, Eq. (3.3) is transformed to

$$\Theta^q \mathbf{U}^q + \Xi^q \mathbf{U} = \Upsilon^q \mathbf{T},$$

in which

$$\begin{aligned}
\mathbf{U}^q &= \begin{bmatrix} u_{q1} & u_{q2} \end{bmatrix}^{\mathrm{T}}, \\
\mathbf{U} &= \begin{bmatrix} u_{11} & u_{12} & u_{21} & u_{22} & \dots & u_{n_p1} & u_{n_p2} \end{bmatrix}^{\mathrm{T}}, \\
\mathbf{T} &= \begin{bmatrix} t_{11} & t_{12} & t_{21} & t_{22} & \dots & t_{n_p1} & t_{n_p2} \end{bmatrix}^{\mathrm{T}}, \\
\Theta^q &= \begin{bmatrix} \Theta^q_{11} & \Theta^q_{12} \\ \Theta^q_{21} & \Theta^q_{22} \end{bmatrix}, \\
\Xi^q &= \begin{bmatrix} \Xi^{1q}_{11} & \Xi^{1q}_{12} & \Xi^{2q}_{11} & \Xi^{2q}_{12} & \dots & \Xi^{n_pq}_{11} & \Xi^{n_pq}_{12} \\ \Xi^{1q}_{21} & \Xi^{1q}_{22} & \Xi^{2q}_{21} & \Xi^{2q}_{22} & \dots & \Xi^{n_pq}_{21} & \Xi^{n_pq}_{22} \end{bmatrix}, \\
\Upsilon^q &= \begin{bmatrix} \Upsilon^{1q}_{11} & \Upsilon^{1q}_{12} & \Upsilon^{2q}_{11} & \Upsilon^{2q}_{12} & \dots & \Upsilon^{n_pq}_{11} & \Upsilon^{n_pq}_{12} \\ \Upsilon^{1q}_{21} & \Upsilon^{1q}_{22} & \Upsilon^{2q}_{21} & \Upsilon^{2q}_{22} & \dots & \Upsilon^{n_pq}_{21} & \Upsilon^{n_pq}_{22} \end{bmatrix}, \\
\Xi^{pq}_{ij} &= \sum_{m=1}^{N} \int_{\Gamma_m} t^*_{ij}(\vartheta_q, \mathbf{x}) \phi_p(\mathbf{x}) d\Gamma, \\
\Upsilon^{pq}_{ij} &= \sum_{m=1}^{N} \int_{\Gamma_m} u^*_{ij}(\vartheta_q, \mathbf{x}) \phi_p(\mathbf{x}) d\Gamma.
\end{aligned}$$

Thus, for all nodes, we can get

$$\Theta \mathbf{U} + \Xi \mathbf{U} = \Upsilon \mathbf{T},$$

in which

$$\Theta = \begin{bmatrix} \Theta^1 & 0 & \dots & 0 \\ 0 & \Theta^1 & \dots & 0 \\ \vdots & \vdots & \ddots & \vdots \\ 0 & 0 & \dots & \Theta^{n_p} \end{bmatrix},$$

$$\Xi = \begin{bmatrix} \Xi^1 & \Xi^2 & \dots & \Xi^{n_p} \end{bmatrix}^{\mathrm{T}},$$

$$\Upsilon = \begin{bmatrix} \Upsilon^1 & \Upsilon^2 & \dots & \Upsilon^{n_p} \end{bmatrix}^{\mathrm{T}}.$$

4. Numerical results

In this part of paper, we test the proposed new technique on four test problems. The used plate or in other word the computational domains are non-rectangular that show the efficiency of the present method. We employ the **Matlab** 7 software based on version of 2010 with 4 Gbyte of memory. In numerical examples, we employ four complex domains that are shown in Figure 1.

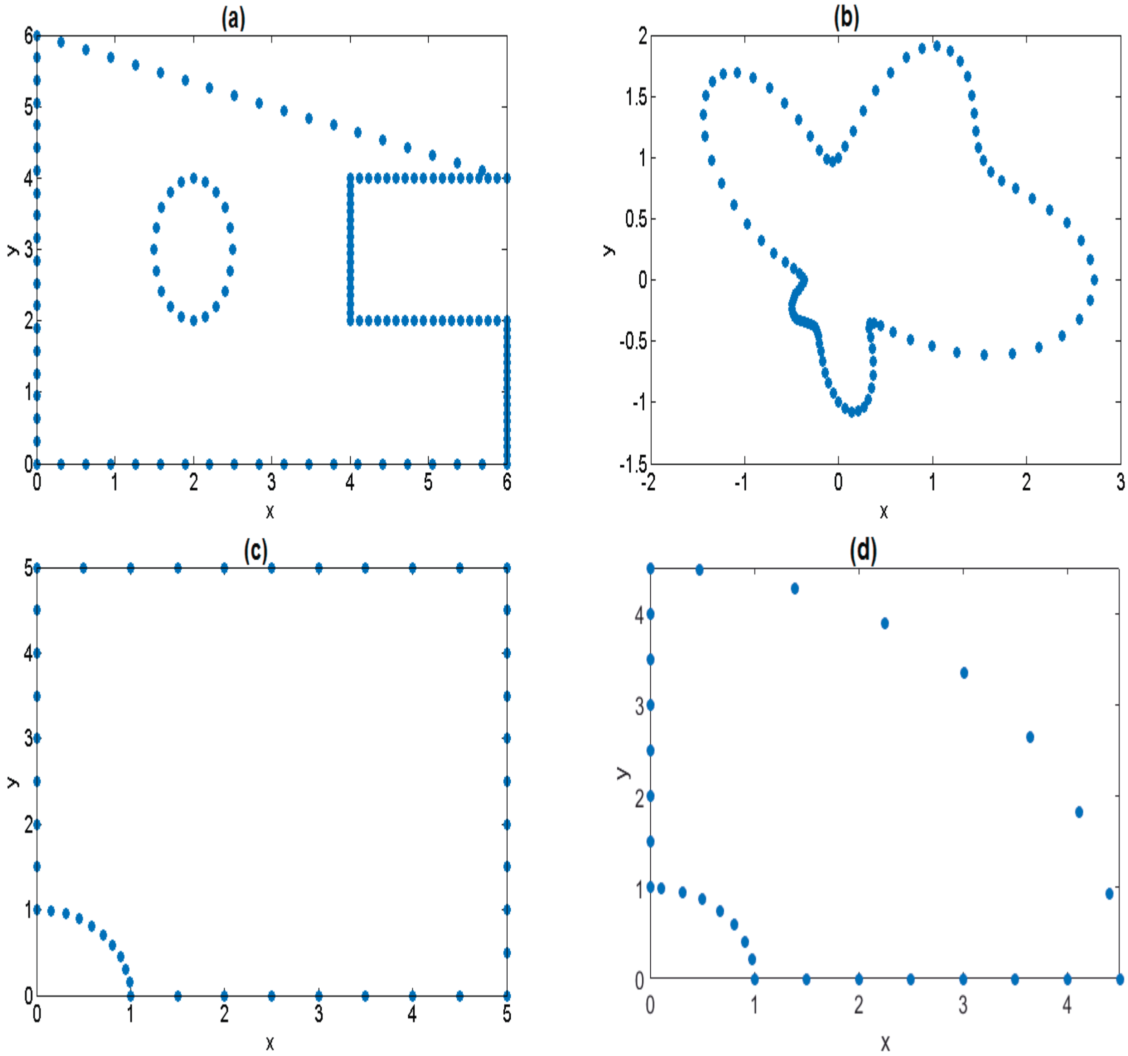

Figure 1: The considered computational domains

4.1. A cantilevered beam

At first, we consider a cantilevered beam with its left end fixed. Figure 2 shows the free end of the beam is subjected to a parabolic downward traction. The analytical solutions of the displacement components are [50]

$$\begin{aligned} u_1 &= -\frac{Py}{6EI}\left[(6L-3x)x+(2+v)\left(y^2-\frac{D^2}{4}\right)\right], \\ u_2 &= \frac{P}{6EI}\left[3vy^2(L-x)+(4+5v)\frac{D^2x}{4}+(2L-x)\,x^2\right], \end{aligned}$$

in which

- moment of inertia is $I=\dfrac{D^3}{12}$,
- Poisson's ratio $v=0.3$,
- Young's modulus $E=30$ MPa.

Also, the stress components that correspond to the foregoing displacements are

$$\sigma_1=-\frac{P(L-x)y}{I}, \qquad \sigma_2=0, \qquad \sigma_{12}=\frac{P}{2I}\left(\frac{D^2}{4}-y^2\right),$$

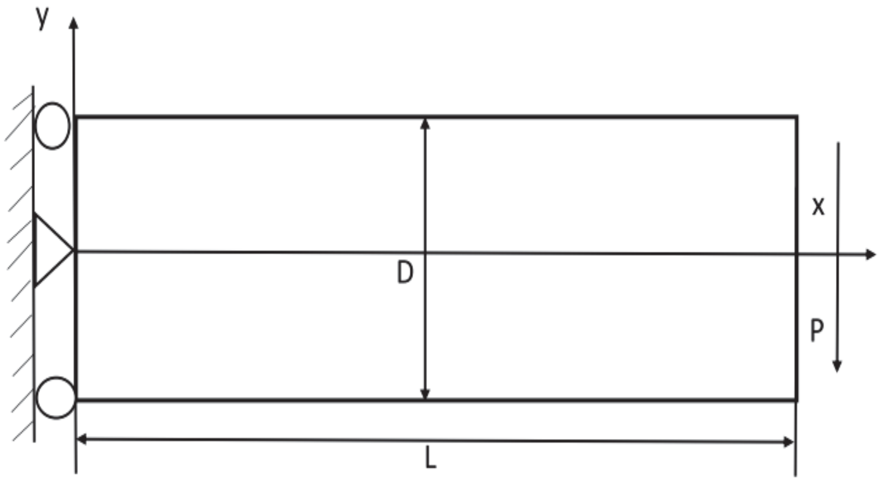

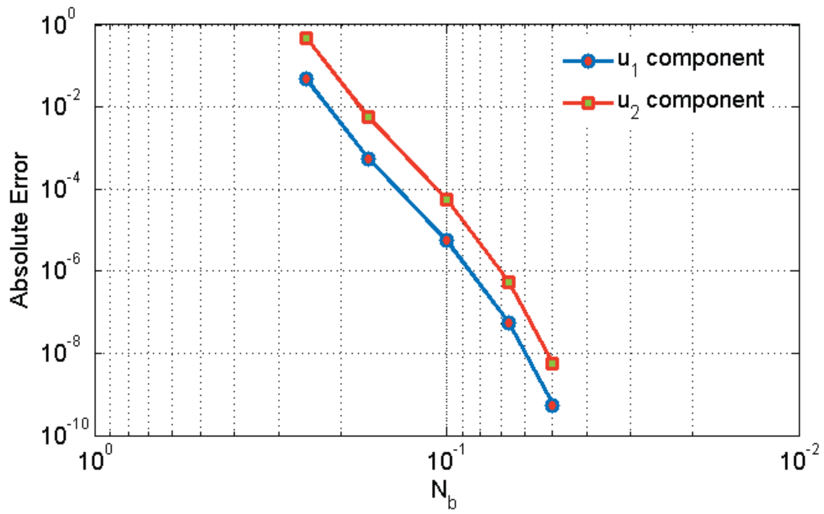

Figure 3: The obtained errors as a function for a different number of boundary nodes for Example 1.

in which $P = 10^3$ N, the length of domain is $L = 50$ mm and the width of the beam is $D = 10$ mm. We would like to solve this problem using the new technique proposed in the current work. We select $\epsilon = 0.001$ and use different numbers for boundary node to simulate Example 1 on a square plate where the obtained results are depicted in Figure 3. Also, we consider Figure 1 part (a) as the computational domain and obtain the results for it with $N_b = 10$ and $N_b = 15$ based on different values of ϵ where the results are presented in Figure 4. As well as, in Table 1 the obtained results using the method presented in the current article are compared with the developed method in [50].

Table 1

Comparison between the method of [50] and the present method

	Method of [50]		Present method			
N	Displacement	Stress	N_b	Displacement	Stress	time(s)
9×7	7.095×10^{-3}	2.663×10^{-2}	4	4.581×10^{-5}	7.735×10^{-4}	3.21
17×13	7.469×10^{-4}	6.411×10^{-3}	6	2.710×10^{-5}	3.009×10^{-4}	7.50
25×19	1.924×10^{-4}	3.775×10^{-3}	8	8.079×10^{-6}	1.491×10^{-4}	13.11
33×19	1.191×10^{-4}	2.745×10^{-3}	10	5.188×10^{-6}	8.691×10^{-5}	27.42
33×25	7.548×10^{-5}	2.446×10^{-3}	12	2.310×10^{-6}	4.205×10^{-5}	34.27
41×31	3.672×10^{-5}	1.714×10^{-3}	14	9.714×10^{-7}	2.196×10^{-5}	54.77

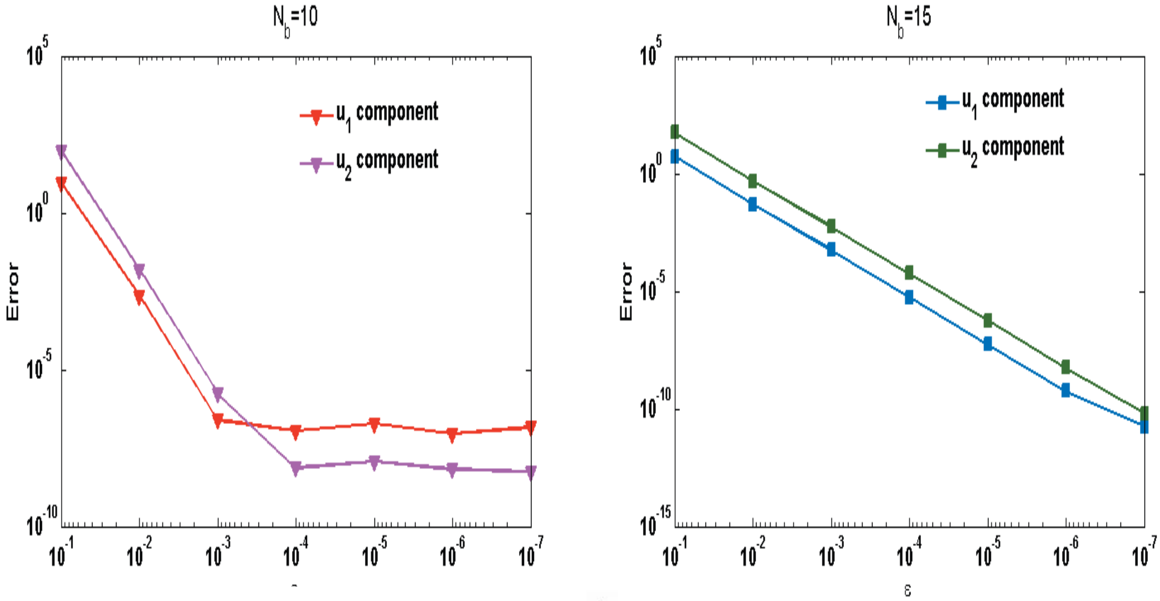

Figure 4: The obt Ω_1 for Example 1 .

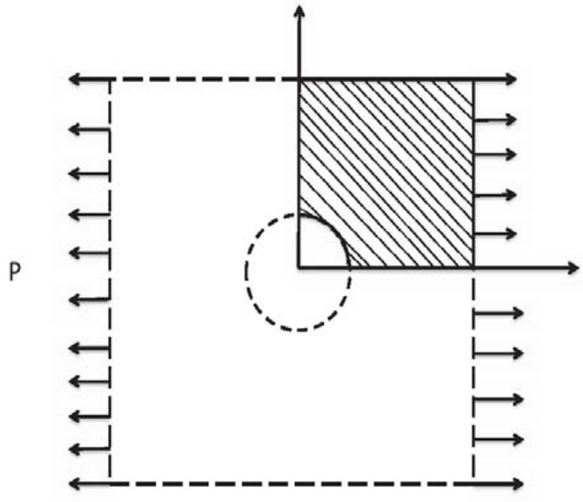

Figure 5: A rectangular plate with a hole subjected to a distributed load.

4.2. A square plate with a central circular hole

For the second example, a square plate with a central circular hole is considered that is depicted in Figure 5. The exact solutions for the stresses are [50]

$$
\begin{aligned}
\sigma_{11}(r,\theta) &= q\left\{1-\frac{a^2}{r^2}\left[\frac{3}{2}\cos(2\theta)+\cos(2\theta)\right]+\frac{3}{2}\frac{a^4}{r^4}\cos(4\theta)\right\},\\
\sigma_{22}(r,\theta) &= q\left\{\frac{a^2}{r^2}\left[\frac{1}{2}\cos(2\theta)-\cos(4\theta)\right]+\frac{3}{2}\frac{a^4}{r^4}\cos(4\theta)\right\},\\
\tau_{12}(r,\theta) &= -q\left\{\frac{a^2}{r^2}\left[\frac{1}{2}\sin(2\theta)+\sin(4\theta)\right]-\frac{3}{2}\frac{a^4}{r^4}\sin(4\theta)\right\}.
\end{aligned}
$$

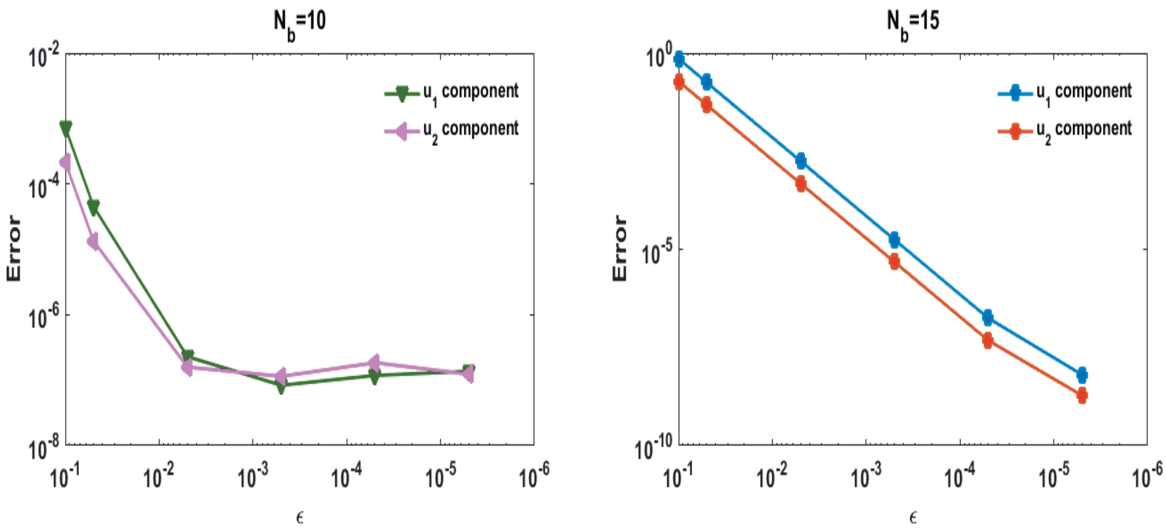

Figure 6: The obtained errors as a function for different values of ϵ on domain Ω_1 for Example 2.

Also, the analytical solutions for the displacements are

$$u_r(r,\theta) = \frac{q}{4E}\left\{ r\left[\frac{k-1}{2} + \cos(2\theta)\right] + \frac{a^2}{r}\left[1+(1+k)\cos(2\theta)\right] - \frac{a^4}{r^3}\cos(2\theta)\right\},$$

$$u_\theta(r,\theta) = \frac{q}{4E}\left[(1-k)\frac{a^2}{r} - r - \frac{a^4}{r^3}\right]\sin(2\theta),$$

in which

$$k = \begin{cases} 3-4v, & \text{plane strain} \\ \dfrac{3-v}{1+v}, & \text{plane stress} \end{cases},$$

and (r,θ) are the polar coordinates. In this case, plane strain condition is assumed and the material properties are $E = 2.0 \times 10^5$ MPa and $v = 0.25$. Symmetry conditions are imposed on the left and bottom edges and also the inner boundary of the hole is traction free.

Table 2
Comparison between the method of [50] and the present method

	Method of [50]		Present method			
N	Displacement	Stress	N_b	Displacement	Stress	time(s)
5×11	3.264×10^{-4}	2.663×10^{-1}	4	1.381×10^{-5}	4.251×10^{-3}	2.33
6×11	2.879×10^{-4}	6.411×10^{-1}	6	1.169×10^{-5}	3.509×10^{-3}	8.67
7×11	3.160×10^{-4}	3.775×10^{-1}	8	8.905×10^{-6}	9.183×10^{-4}	15.93
8×11	2.870×10^{-4}	2.745×10^{-2}	10	3.991×10^{-6}	7.601×10^{-4}	27.77
9×11	8.651×10^{-5}	2.446×10^{-2}	12	1.073×10^{-6}	3.131×10^{-4}	40.13

We consider Figure 1 part (b) as the computational domain and obtain the results for it with $N_b = 10$ and $N_b = 15$ based on the different values of ϵ where the results are presented in Figure 6. Also, in Table 2 the obtained results using the method presented here are compared with the developed method in [50].

4.3. Internal and external pressurized hollow cylinder

For the third example, a hollow cylinder under internal pressure is considered similar to Figure 8. The analytical solutions are [50]

$$\begin{aligned}
\sigma_r &= \frac{a^2b^2(P_b - P_a)}{b^2-a^2}\cdot\frac{1}{r^2} + \frac{a^2P_a - b^2P_b)}{b^2-a^2},\\
\sigma_\theta &= -\frac{a^2b^2(P_b - P_a)}{b^2-a^2}\cdot\frac{1}{r^2} + \frac{a^2P_a - b^2P_b)}{b^2-a^2},\\
u_r &= \frac{1}{E}\left\{(1-v)\frac{a^2P_a - b^2P_b)}{b^2-a^2}\cdot r - (1+v)\frac{a^2b^2(P_b - P_a)}{b^2-a^2}\cdot\frac{1}{r}\right\},\\
u_\theta &= 0,
\end{aligned}$$

in which $v = 0.25$, $a = 1$ and $b = 5$. We apply the new method for solving this problem. We select $\epsilon = 0.0001$ and use different numbers for boundary node to simulate Example 3 on a hollow cylinder under internal pressure and the obtained results are compared with method presented in [50] also these results are shown in Table 3. Also, we consider Figure 1 parts (c) and (d) as the computational domain and obtain the results for it with $N_b = 10$ and $N_b = 15$ based on the different values of ϵ where the results are demonstrated in Figure 7.

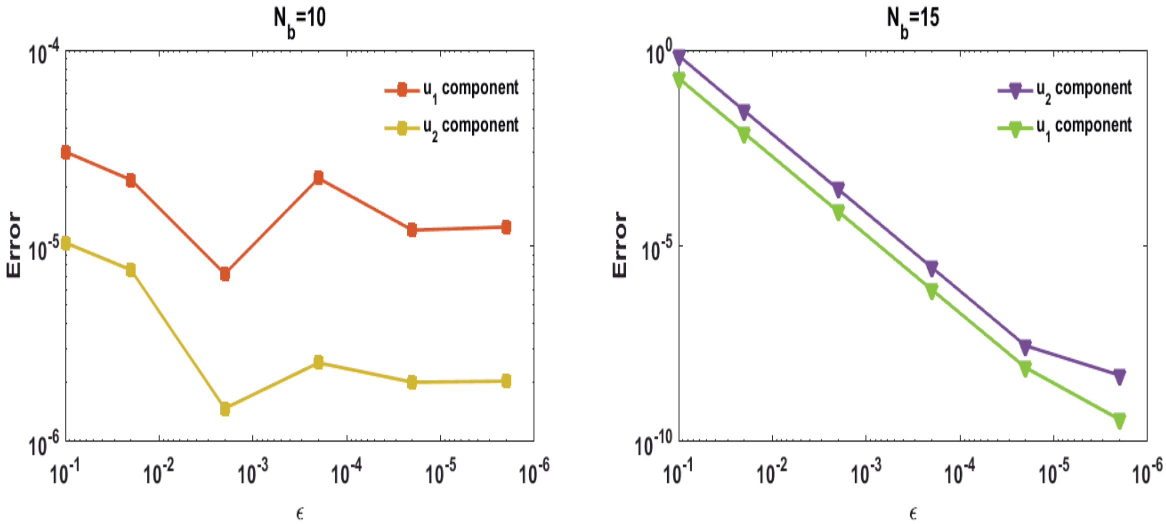

Figure 7: The obtained errors as a function for different values of ϵ on domain of part (c) (left panel) and part (d) (right panel) for Example 3.

Table 3
Comparison between the method of [50] and the present method

	Method of [50]		Present method		
N	Displacement	Stress	N_b	Displacement	Stress
8×11	2.176×10^{-3}	7.262×10^{-2}	4	1.760×10^{-5}	7.761×10^{-5}
9×11	1.539×10^{-3}	4.731×10^{-2}	6	1.023×10^{-5}	5.490×10^{-5}
10×11	4.879×10^{-4}	2.374×10^{-2}	8	8.039×10^{-6}	2.340×10^{-5}
11×11	3.862×10^{-4}	9.013×10^{-3}	10	5.398×10^{-6}	1.219×10^{-5}

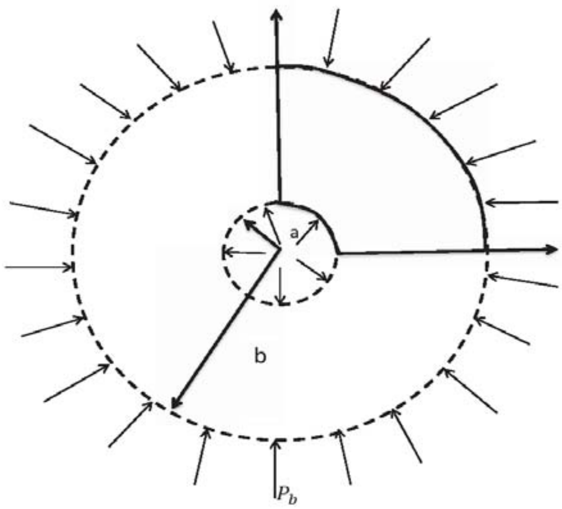

Figure 8: A rectangular plate with a hole subjected to a distributed load.

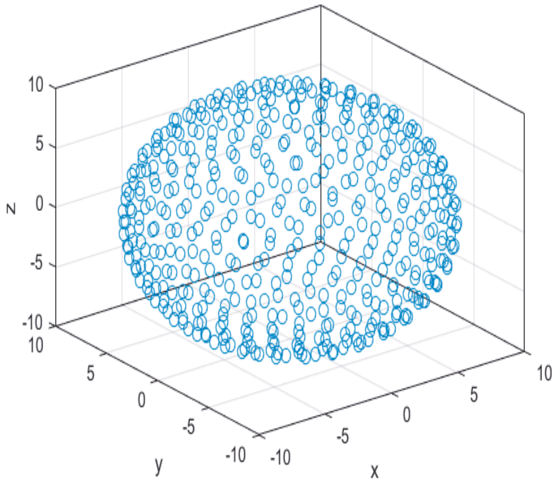

Figure 9: The consideration domain and meshless points in Boussinesq problem.

4.4. 3D Boussinesq problem

We consider the Boussinesq problem which is described as a concentrated load acting on a semi-finite elastic medium with no body force. For this example, the exact displacement field is [46]

$$u_r = \frac{(1+\nu)P}{2E\pi\rho}\left[\frac{zr}{\rho^2} - \frac{(1-2\nu)r}{\rho+z}\right],$$

$$w = \frac{(1+\nu)P}{2E\pi\rho}\left[\frac{z^2}{\rho^2} + 2(1-\nu)\right],$$

in which

1. u_r is the radial displacement,
2. w is the vertical displacement,
3. $\rho = \sqrt{x_1^2 + x_2^2 + x_3^2}$ is the distance to the loading point,
4. $r = \sqrt{x_1^2 + x_2^2}$ is the projection of ρ on the loading surface.

Then the exact stresses are

$$\sigma_r = \frac{P}{2\pi\rho^2}\left[-\frac{3zr}{\rho^3} - \frac{(1-2\nu)\rho}{\rho+z}\right],$$

$$\sigma_\theta = \frac{(1-2\nu)P}{2\pi\rho^2}\left[\frac{z}{\rho} - \frac{\rho}{\rho+z}\right],$$

$$\sigma_{zz} = -\frac{3\pi z^3}{2\pi\rho^5},$$

$$\tau_{zr} = \tau_{rz} = -\frac{3\pi r z^2}{2\pi\rho^5}.$$

We solve this problem using the proposed technique.

Table 4

Error obtained using the present method with different values of shape functions

	$\epsilon = 0.01$		$\epsilon = 0.005$	
N	u_r	w	u_r	w
$6\times6\times6$	8.2511×10^{-2}	7.0189×10^{-2}	6.2813×10^{-2}	5.8101×10^{-2}
$8\times8\times8$	3.8017×10^{-2}	3.1389×10^{-2}	1.4513×10^{-2}	1.0019×10^{-2}
$10\times10\times10$	9.2589×10^{-3}	8.7880×10^{-3}	7.9013×10^{-3}	5.1961×10^{-3}
$12\times12\times12$	4.9809×10^{-3}	3.6918×10^{-3}	2.2813×10^{-3}	1.7315×10^{-3}
$14\times14\times14$	9.4511×10^{-4}	9.0180×10^{-4}	5.5541×10^{-4}	4.8189×10^{-4}

Table 4 shows the error obtained using the boundary node method based on the RBF-QR approach for different values of shape parameter ϵ.

5. Conclusion

In the current paper, the boundary element method has been combined with the RBF-QR approach. The boundary element method can be classified in the meshless methods in which to simulate the considered problem, we need to set some nodes in the boundary problem. The shape functions of RBF-QR approach have spectral accuracy for small shape parameters. Thus, we combined the boundary element method with the RBF-QR technique and obtained a high accuracy version of the boundary element method. We checked the new numerical algorithm for solving the multi-dimensional elasticity problems on non-rectangular plates. Numerical results confirm the efficiency of the new method developed in the current paper.

Acknowledgment:

The authors are grateful to the reviewers for carefully reading this paper and for their comments and suggestions which really have improved the paper.

References

[1] T. Belytschko, Y. Krongauz, D. Organ, M. Fleming, P. Krysl, Meshless method: an overview and recent developments, Comput. Methods Appl. Mech. Eng., 139 (1996) 3-47.

[2] J. S. Chen, C. Pan, C.T. Wu, W.K. Liu, Reproducing kernel particle methods for large deformation analysis of non-linear structures, Comput. Methods Appl. Mech. Eng., 139 (1996) 195-227.

[3] L. Chen, Y. M. Cheng, The complex variable reproducing kernel particle method for bending problems of thin plates on elastic foundations, Computational Mechanics, 62 (2018) 67-80.

[4] Y. M. Cheng, F. Bai, C. Liu, M. Peng, Analyzing nonlinear large deformation with an improved element-free Galerkin method via the interpolating moving least-squares method, International Journal of Computational Materials Science and Engineering, 5 (2016) 1650023.

[5] Y. M. Cheng, C. Liu, F. N. Bai, M. J. Peng, Analysis of elastoplasticity problems using an improved complex variable element-free Galerkin method, Chinese Physics B, 24 (2015)

[6] M. Dehghan, M. Abbaszadeh, A local meshless method for solving multi-dimensional Vlasov-Poisson and Vlasov-Poisson–Fokker–Planck systems arising in plasma physics, Engineering with Computers, 33 (2017) 961-981.

[7] M. Dehghan, M. Abbaszadeh, Proper orthogonal decomposition variational multiscale element free Galerkin (POD-VMEFG) meshless method for solving incompressible Navier–Stokes equation, Computer Methods in Applied Mechanics and Engineering, 311 (2016) 856-888.

[8] M. Dehghan, M. Abbaszadeh, An upwind local radial basis functions-differential quadrature (RBF-DQ) method with proper orthogonal decomposition (POD) approach for solving compressible Euler equation, Engineering Analysis with Boundary Elements 92 (2018) 244-256.

[9] M. Dehghan, H. Hosseinzadeh, Calculation of 2D singular and near singular integrals of boundary elements method based on the complex space C, Applied Mathematical Modelling, 36 (2012) 545-560.

[10] M. Dehghan, H. Hosseinzadeh, Improvement of the accuracy in boundary element method based on high-order discretization, Computers & Mathematics with Applications, 62 (2011) 4461-4471.

[11] M. Dehghan, H. Hosseinzadeh, Obtaining the upper bound of discretization error and critical boundary integrals of circular arc boundary element method, Mathematical and Computer Modelling, 55 (2012) 517-529.

[12] W. Elleithy, Analysis of problems in elasto-plasticity via an adaptive FEM-BEM coupling method, Comput. Methods Appl. Mech. Eng., 197 (2008) 3687-3701.

[13] B. Fornberg, E. Larsson, N. Flyer, Stable computations with Gaussian radial basis functions, SIAM J. Sci. Comput., 33 (2011) 869-892.

[14] R. Gowrishankar, S. Mukherjee, A pure boundary node method for potential theory, Commun. Numer. Meth. Eng. 18 (2002) 411-427.

[15] S. Jun, W.K. Liu, T. Belytschko, Explicit reproducing kernel particle methods for large deformation problems, Int. J. Numer. Methods Eng. 41 (1998) 137- 166.

[16] S. J. Kim, J. T. Oden, Finite element analysis of a class of problems in finite elastoplasticity based on the thermodynamical theory of materials of type N, Comput. Methods Appl. Mech. Eng., 53 (1985) 277-302.

[17] E. Larsson, E. Lehto, A. Heryudono, B. Fornberg, Stable computation of differentiation matrices and scattered node stencils based on Gaussian radial basis functions, SIAM J. Sci. Comput. 35(4) (2013) A2096-A2119.

[18] D. M. Li, K. M. Liew, Y. M. Cheng, An improved complex variable element-free Galerkin method for two-dimensional large deformation elastoplasticity problems, Comput. Methods Appl. Mech. Eng., 269 (2014) 72-86.

[19] X. Li, J. Zhu, On a Galerkin boundary node method for potential problems, Advances in Engineering Software, 42 (2011) 927-933.

[20] X. Li, J. Zhu, A Galerkin boundary node method and its convergence analysis, J. Comput. Appl. Math., 230 (2009) 314-328.

[21] X. Li, Meshless analysis of two-dimensional Stokes flows with the Galerkin boundary node method, Eng. Anal. Bound. Elem., 34 (2010) 79-91.

[22] X. Li, S. Li, Meshless boundary node methods for Stokes problems, Appl. Math. Model., 39 (2015) 1769-1783.

[23] X. Li , A meshless interpolating Galerkin boundary node method for Stokes flows, Eng. Anal. Bound. Elem., 51 (2015) 112-122.

[24] K. M. Liew, Y. Cheng, S. Kitipornchai, Boundary element-free method (BEFM) for two-dimensional elastodynamic analysis using Laplace transform, Int. J. Numer. Meth. Eng., 64 (2005) 1610-1627.

[25] G. R. Liu, Y. T. Gu, An Introduction to Meshfree Methods and Their Programming, Springer Science & Business Media, 2005.

[26] G. R. Liu, Meshfree Methods: Moving Beyond the Finite Element Method, Taylor & Francis, 2009.

[27] G. R. Liu, G. Y. Zhang, Upper bound solution to elasticity problems: A unique property of the linearly conforming point interpolation method (LC-PIM), Int. J. Numer. Meth. Eng., 74 (2008) 1128-1161.

[28] W. K. Liu, S. Jun, Multiple-scale reproducing kernel particle methods for large deformation problem, Int. J. Numer. Methods Eng., 41 (1998) 1339-1362.

[29] J. H. Lv, Y. Miao, H. P. Zhu, Boundary node method based on parametric space for 2D elasticity, Eng. Anal. Bound. Elem., 37 (2013) 659-665.

[30] H. P. Ren, Y. M. Cheng, W. Zhang, An interpolating boundary element-free method (IBEFM) for elasticity problems, Physics, Mechanics & Astronomy, 53 (2010) 758-766.

[31] Z. J. Meng, H. Cheng, L. D. Ma, Y. M. Cheng, The dimension split element-free Galerkin method for three-dimensional potential problems, Acta Mechanica Sinica/Lixue Xuebao, 34(3) (2018) 462-474.

[32] Miao Yu, W. Yuan-han, Meshless analysis for three-dimensional elasticity with singular hybrid boundary node method, Appl. Math. Mech., 27 (2006) 673–681.

[33] D. Mirzaei, A new low-cost meshfree method for two and three dimensional problems in elasticity, Appl. Math. Model., 39 (2015) 7181-7196.

[34] Y. X. Mukherjee, S. Mukherjee, The boundary node method for potential problems, Int. J. Numer. Meth. Eng., 40 (1997) 797-815.

[35] M. Peng, D. Li, Y. M. Cheng, The complex variable element-free Galerkin (CVEFG) method for elasto-plasticity problems, Engineering Structures, 33 (2011) 127-135.

[36] M. Tezer-Sezgin, Boundary element method solution of MHD flow in a rectangular duct, Internat. J. Numer. Methods Fluids, 18 (1994) 937-952.

[37] M. Tezer-Sezgin, S. Han Aydin, Solution of magnetohydrodynamic flow problems using the boundary element method, Eng. Anal. Bound. Elem., 30 (2006) 411-418.

[38] M. Tezer-Sezgin, C. Bozkaya, Boundary element method solution of magnetohydrodynamic flow in a rectangular duct with conducting walls parallel to applied magnetic field, Comput. Mech., 41 (2008) 769-775.

[39] M. Tezer-Sezgin, C. Bozkaya, The boundary element solution of magnetohydrodynamic flow in an infinite region, J. Comput. Appl. Math., 225 (2009) 510-521.

[40] J. Sladek, V. A. Sladek, A meshless method for large deflection of plates, Comput. Mech. 30 (2) (2003) 155-163.

[41] F. Sun, J. Wang, Y. M. Cheng, An improved interpolating element-free Galerkin method for elasticity, Chinese Physics B, 22(12) (2013) 120203.

[42] F. Sun, J. Wang, Y.M.Cheng, A. Huang, Error estimates for the interpolating moving least-squares method in n-dimensional space, Applied Numerical Mathematics, 98 (2015) 79-105.

[43] F. Tan, Y. Zhang, Y. Li, Development of a meshless hybrid boundary node method for Stokes flows, Eng. Anal. Bound. Elem. 37 (2013) 899-908.

[44] F. Tan, Y. Zhang, Y. Li, An improved hybrid boundary node method for 2D crack problems, Archive of Applied Mechanics, 85 (2015) 101-116.

[45] M. Tatari, F. Ghasemi, The Galerkin boundary node method for magneto-hydrodynamic (MHD) equation, J. Comput. Phys. 258 (2014) 634-649.

[46] S. P. Timoshenko, J. N. Goodier, Theory of Elasticity, third ed., McGraw-Hill, New York, 1970.

[47] J. Wang, J. Wang, F. Sun, Y. M. Cheng, An interpolating boundary element-free method with nonsingular weight function for two-dimensional potential problems, International Journal of Computational Methods, 10 (2013) 1350043.

[48] H. Xie, T. Nogami, J. Wang, A radial boundary node method for two-dimensional elastic analysis, Eng. Anal. Bound. Elem., 27 (2003) 853-862.

[49] F. Yan, X. T. Feng, H. Zhou, Dual reciprocity hybrid radial boundary node method for the analysis of Kirchhoff plates, Appl. Math. Model. 35 (2011) 5691-5706.

[50] L. W. Zhang, K. M. Liew, An improved moving least-squares Ritz method for two-dimensional elasticity problems, Appl. Math. Comput., 246 (2014) 268-282.

[51] J. Zhang, Z. Yao, H. Li, A hybrid boundary node method, Int. J. Numer. Meth. Eng., 53 (2002) 751-763.

[52] Y. M. Zhang, F. L. Sun, D. L. Young, W. Chen, Y. Gud, Average source boundary node method for potential problems, Eng. Anal. Bound. Elem. 70 (2016) 114-125.

Please cite this article using:

Mostafa Abbaszadeh*, Mehdi Dehghan, A meshless numerical investigation based on the RBF-QR approach for elasticity problems, AUT J. Math. Com., 1(1) (2020) 1-15
DOI: 10.22060/ajmc.2019.15990.1019